Journal of Magnetism and Magnetic Materials 399 (2016) 199–206

Contents lists available at ScienceDirect

Journal of Magnetism and Magnetic Materials

journal homepage: www.elsevier.com/locate/jmmm

Static and dynamic magnetic properties of Co_2FeAl-based stripe arrays

M. Belmeguenai [a,*], M.S. Gabor [b], F. Zighem [a], D. Berling [c], Y. Roussigné [a], T. Petrisor Jr. [b], S.M. Chérif [a], C. Tiusan [b,d], O. Brinza [a], P. Moch [a]

[a] LSPM-CNRS, Université Paris XIII-Sorbonne Paris Cité, 93430 Villetaneuse, France
[b] Center for Superconductivity, Spintronics and Surface Science, Technical University of Cluj-Napoca, Str. Memorandumului No. 28 RO-400114, Cluj-Napoca, Romania
[c] IS2M, CNRS-LRC 7228, Université de Haute-Alsace, 68057 Mulhouse-Cedex, France
[d] Institut Jean Lamour, CNRS, Université de Nancy, BP 70239, F-54506 Vandoeuvre, France

ARTICLE INFO

Article history:
Received 30 June 2015
Received in revised form
16 September 2015
Accepted 21 September 2015
Available online 25 September 2015

Keywords:
Magnetization dynamics
Magnetic anisotropy
Ferromagnetic resonance (FMR)
Spin waves
Nanostructures

ABSTRACT

25 nm to 50 nm Co_2FeAl (CFA) thick wire arrays with varying widths and spacing have been patterned from continuous CFA films deposited on MgO(001) using e-beam lithography and Ar ion milling. Magneto-optical Kerr effect, transverse bias initial inverse susceptibility and torque measurements reveal that the in-plane magnetic anisotropy of the wires is dominantly monitored by a uniaxial term, in contrast with the continuous films where it is governed by the superposition of a fourfold term and of a smaller uniaxial term. The microstrip ferromagnetic resonance spectra performed using a magnetic field H, applied in the plane of the studied sample along various directions, or perpendicularly to this plane, gave us access to various quantized modes originating from the patterning. In addition, Brillouin light scattering also exhibits quantized modes. A large part of the experimental observations can be quantitatively interpreted as resulting from the demagnetizing terms induced by the geometrical patterning. However, the presented model, simply built on the effect of the demagnetizing field, is not able to give account of all the quantized modes present in the resonance spectra. When H is parallel to the wires, a more complete description is used: it considers the wave-vector quantization induced by the patterning. For the magnetic modes concerned by both approaches, the correspondence between the 2 models is easily established. When H is not parallel to the wires quantitative descriptions of the behavior of the field dependence of the observed modes still can often be performed. Finally, in all the studied patterned samples, the uniform magnetic mode, termed "film mode", relative to the parent continuous film is observed by ferromagnetic resonance: such a behavior, which has been reported previously, remains to be completely interpreted.

1. Introduction

Spintronics is, nowadays, facing challenges such as spin injection into semiconductors [1,2], obtaining high magnetoresistance values and low current density for spin transfer-based devices [3]. Highly spin polarized materials with low Gilbert damping parameter such as Co-based Heusler alloys are good candidates to overcome these difficulties. Co_2FeAl (CFA) is one of the most prominent Co-based Heusler [4] alloys. Its Curie temperature is very high (1000 K), and this alloy is theoretically predicted to be half-metallic, thus yielding a full spin polarization. It can provide giant tunneling magnetoresistance (360% at room temperature) [5], when used as an electrode in magnetic tunnel junctions. Consequently CFA is promising for practical applications. The storage density in continuous magnetic media is, nowadays, limited by the superparamagnetic effect. Nano-patterned media are expected to significantly increase the super-paramagnetic limit [6]. However, the high frequency magnetization dynamics in nano-objects is related to non-uniform spin wave modes in contrast to the almost uniform precession of magnetization in continuous thin films. Therefore, the knowledge of the high frequency dynamics of submicronic magnetic systems is of critical importance both for fundamental and technological reasons. Indeed, in view of the potential applications in magnetic recording and smart sensors technology [7,8], the magnetization dynamics of nano-objects is critically important for the understanding and the improvement of the noise and magnetization reversal characteristics. It defines the timescale of the magnetization reversal process, and therefore, the switching time of a memory unit.

From the fundamental point of view, both the size and the spatial arrangement of these nanostructures significantly influence their magnetic properties, leading to the appearance of new

* Corresponding author.
E-mail address: belmeguenai.mohamed@univ-paris13.fr (M. Belmeguenai).

http://dx.doi.org/10.1016/j.jmmm.2015.09.065
0304-8853/

physical phenomena not existing in the continuous films. The size reduction of the structures can lead to new interesting phenomena: the geometrical confinement induces a quantization of the spin waves [9,10], giving rise to magnonic bands [11,12] showing a dispersion versus their wave-vector which depends on the periodical arrangement of the studied array. The spin waves confinement has usually been probed using Brillouin light scattering (BLS) [13–17]. Ferromagnetic resonance (FMR) is another technique, up to now less used to study these effects [18,19]. The FMR presents several advantages compared to the BLS. Indeed, the FMR provides high accuracy in determining the positions of the resonance peaks, which results from much higher resolution in the determination of natural frequencies of the studied system. In addition, FMR experiments with a magnetic field applied perpendicular to the plane of the studied nanostructures are easier than the BLS ones. Moreover, due to its small damping values [20] providing a much longer FMR coherent length, CFA is much more suitable for magnonic devices and therefore, the high frequency magnetization dynamics of CFA-based nanostructures is of important research interest. In this paper, we mainly used ferromagnetic resonance in microstrip line (MS-FMR) under in-plane and out-of-plane applied magnetic fields, combined with magneto-optical Kerr effect magnetometry and BLS spectroscopy, in order to perform a complete correlated analysis pointing out striking effects related to the size reduction of Co_2FeAl based arrays of wires. We show that the reduction in size of our samples leads principally to quantization effects, which change dramatically the spin waves spectrum, compared to that of continuous films.

2. Samples preparation and experimental methods

To observe the quantization and to facilitate the interpretation of the of spin waves spectra, the thickness d of the studied samples must be well chosen. It has to be large enough in order to insure that the frequencies of the quantized modes resulting from the patterning significantly differ from the frequency of the continuous film and small enough in order to avoid strong interaction between the magnetic excitations arising from the uniform mode of the continuous film and the perpendicular standing spin waves (PSSW). Therefore, thicknesses in the range 20–50 nm are an optimum choice for spin waves quantizing study.

CFA films were grown on MgO(001) single-crystal substrates using a magnetron sputtering system with a base pressure lower than 3×10^{-9} Torr. Prior to the deposition of the CFA films, a 4 nm thick MgO buffer layer was grown at room temperature (RT) by radio frequency sputtering from a MgO polycrystalline target under an Argon pressure of 15 mTorr. Next, the CFA films, with variable thicknesses (25 nm, 43 nm and 50 nm), were deposited at RT by dc sputtering under an Argon pressure of 1 mTorr, at a rate of 0.1 nm/s. Finally, the 25 nm and 50 nm CFA films were capped with a MgO(4 nm)/Cr(10 nm) bilayer while the 43 nm thick CFA film was capped with a MgO(4 nm)/Ta(10 nm) bilayer. After the growth of the stack, the structures were ex situ annealed at 600 °C during 15 min in vacuum (pressure lower than 3×10^{-8} Torr) in order to improve their structural and chemical order [21]. A detailed investigation of the thickness and annealing temperature dependences of the magnetic and the structural properties of the continuous films is presented in [20,21]. $500\times500\ \mu m^2$ wire arrays of different widths W ($0.5\ \mu m \le W \le 2\ \mu m$) and arranged with different spacing distances W ($0.5\ \mu m \le S \le 2\ \mu m$) were then elaborated, as illustrated by the scanning electron microscope image shown in Fig. 1. The thin wire arrays were fabricated using electron beam lithography followed by Ar ion milling through the aluminum mask defined by the lift-off technique.

For the dynamic measurements, microstrip ferromagnetic resonance [20], where the studied sample is mounted on a 0.7 mm microstrip line connected to a vector network analyzer and to a lock-in amplifier, is used The instrumental set-up provides the field first derivative of the absorbed power versus the applied magnetic field. During the measurements, the external magnetic field H can be applied in the film plane, along any chosen direction (e.g.: parallel (Fig. 1: 1) or perpendicular (Fig. 1: 2) to the wires) or perpendicularly to this plane (Fig. 1: 3 and 4) as illustrated in Fig. 1. Depending on the directions of H and of the radiofrequency field (h_{rf}), the above described different configurations are labeled 1, 2, 3 and 4 in the following parts of the paper.

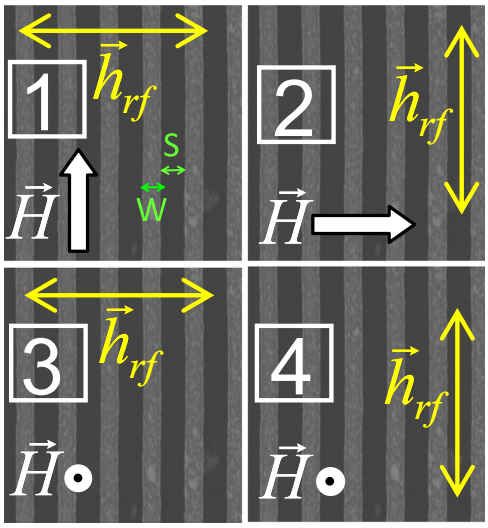

Fig. 1. Scanning electron microscope (SEM) image of an array of Co_2FeAl wires, with a width W spaced of S, illustrating the different configurations used in MS-FMR measurements, where H is the applied static field and h_{rf} is radiofrequency field generated by the microstrip line. The numbers 1, 2, 3 and 4 are used in the text for referring to these configurations. Axes x, y and z are along the wire axis, the wire width and perpendicular the wire plane, respectively.

Magnetization at saturation of the continuous films (found average value: $M_s = 1000 \pm 50$ emu cm^{-3}) and hysteresis loops were studied at room temperature for each sample, using a vibrating sample magnetometer (VSM) and a magneto-optical Kerr effect (MOKE) system, respectively. Moreover, transverse biased initial inverse susceptibility and torque method (TBIIST) [22] was used to study the in-plane anisotropy for comparison with MS-FMR. In addition, X-rays diffraction spectra revealed that the cubic [001] CFA axis is normal to the substrate and that all the CFA films exhibit full epitaxial growth according to the expected CFA(001)[110]//MgO(001)[100] epitaxial relation [20].

3. Synthetic description of static and dynamic magnetic properties

As previously published [20], in the case of a thin CFA film, the frequency of the uniform magnetic mode is easily derived from the expression of the magnetic energy. In the case of an array of wires, this frequency is modified. This variation can be simply interpreted as originating from the demagnetizing field induced by the geometrical transformation of the initial continuous film into such array. Schematically, the components of the effective demagnetizing field derive from the demagnetization coefficients $N_x = 0$, N_y and N_z. Assuming a uniform magnetization, the demagnetizing field inside a wire is easily calculated and depends on the position. At the center of the rectangular section, it is significantly smaller than its average value across the whole section. N_y and N_z depend on d/W and on W/L (where $L = W + S$ is the period of the studied

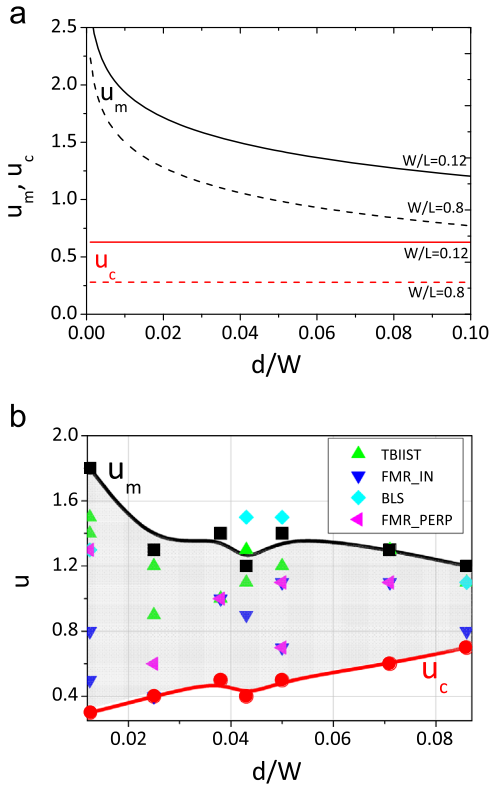

Fig. 2. (a) Evolution of the calculated values of the parameter u at the centre (u_c) and averaged through the wire-section (u_m) as function of d/W for the minimal (0.12) and maximal (0.8) studied coverage ratios W/L. (b) The parameters u extracted from the best fits to the data related arising from the various experimental techniques described in the text; the abscissa axis shows the d/W values used in this work. The experimental data are compared to the (d/W and W/L depending) values of u_m and of u_c calculated for each studied sample. The bold lines are used as eyes guide and the shadowed area is used to clearly show that the experimental data are in the range between u_m and u_c. (For interpretation of the references to color in this figure caption, the reader is referred to the web version of this paper.)

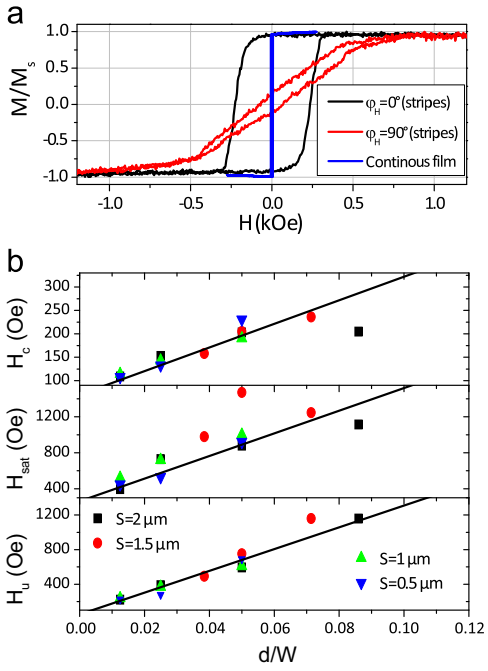

Fig. 3. (a) Typical MOKE hysteresis loops of a 25 nm Co_2FeAl arrays of wires. The in-plane magnetic field is applied parallel ($\varphi_H = 0°$) or perpendicular ($\varphi_H = 90°$) to the wires axis. The easy axis hysteresis loop ($\varphi_H = 0°$: field applied along the [110] CFA axis) of the continuous film is shown for comparison. (b) d/W dependence of the easy axis ($\varphi_H = 0°$) coercive field (H_c), of the saturation field (H_{sat}) along the hard axis ($\varphi_H = 90°$) deduced from hysteresis loops and of the uniaxial anisotropy field (H_u) deduced from TBIIST measurements. Symbols refer to the experimental data and solid lines are fits using the model described in the text with $u=1$ for H_u and H_{sat}; for $H_c$the fit is obtained assuming a proportionality to d/W with a slope equal to $u/5 = 0.2$.

array). If $W/L = 0$ (isolated wire), $N_z = (1 - N_y)$, while this equality remains practically exact for all the studied geometrical conditions. N_y is roughly proportional to d/W and decreases versus W/L. Defining u through Eq. (1), the variation of u is reported in Fig. 2 (a) as a function of d/W for the two extreme values of W/L present in our samples. Its values for all the W/L present in our samples are shown in Fig. 2(b) (red and black symbols), where the bold lines are used as guides for eyes and where the area delimited by these values of u is shadowed

$$N_y = u\left(\frac{d}{W}\right) \quad (\text{and: } N_z \approx 1 - N_y) \tag{1}$$

The coefficient u was calculated assuming two hypotheses: (i) u_c: effective demagnetizing field equal to the obtained value in the center of the wire section or (ii) u_m: averaged value across this section. Notice that, in most of the experimentally studied cases, $d/W \ll 1$: with this condition, u_c is given by a simple expression:

$$u_c \simeq \frac{W}{L}\,\mathrm{cot\,an}\left(\frac{\pi W}{2L}\right) \tag{2}$$

When $W/L \ll 1$: $u_c \approx 2/\pi$.

Concerning u_m, its calculated value lies between 1 and 2 for the studied geometrical conditions. In order to validate the model presented above, we have proceeded to magnetometric MOKE measurements, as described in the following subsection.

3.1. Magnetometric measurements (MOKE)

The demagnetizing field is expected to act as an in-plane anisotropy field $H_u = 4\pi M_s N_y = N_y H_{dem}$: it strongly modifies the hysteresis loops, as shown in Fig. 3a, where the MOKE hysteresis loops for an in-plane magnetic field applied along different orientations (φ_H is the angle between H and the [110] axis of the 25 nm thick CFA sample) are presented. In Fig. 3a, typical hysteresis loops of a 0.5 µm width wire array are compared to the observed one in the continuous film. Using an applied field parallel to the wires ($\varphi_H = 0°$), a square-shaped loop is obtained with a rather high coercive field H_c and a full normalized remanence ($M_r/M_s = 0.99$). In contrast, with an in-plane field applied perpendicular to the wires (along the hard axis y: $\varphi_H = 90°$), the magnetization shows a linear dependence versus the field, up to its saturation occurring near H_u. The TBIIST measurements also allow for deducing the H_u. The coercive field (H_c) deduced from hysteresis loops obtained for a magnetic field applied along the direction of the easy axis, the saturation field along the hard axis (H_{sat}) and the uniaxial anisotropy field (H_u derived from the TBIIST measurements) are shown in Fig. 3b as functions of d/W. Using the above-mentioned value of M_s (1000 emu cm^{-3}), H_u gives access to u. The results are shown in Fig. 2b (green triangles). The observed u values do not significantly differ from the mean calculated parameter u_m (black squares). Finally, as usual, the observed coercive field H_c increases as the anisotropy field but lies well below H_u, as shown in Fig. 3b, where $H_c \sim H_u/5$.

3.2. Ferromagnetic resonance

3.2.1. Magnetic field along the wire axis (configuration 1)

In the case of the magnetic field applied along the wire axis,

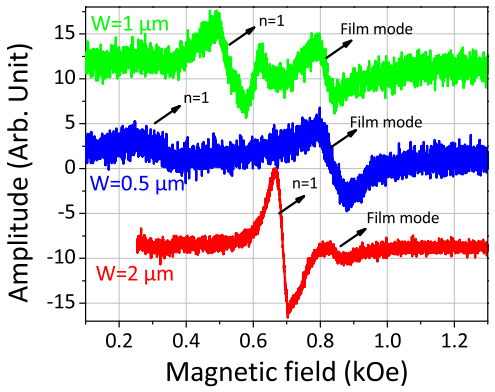

Fig. 4. MS-FMR spectra of 25 nm Co_2FeAl wire arrays of various widths measured at 10.4 GHz driven frequency and for a magnetic field applied along the wire axis. The spectra are shifted vertically for clarity.

3 types of resonance modes can be observed simultaneously in the studied samples as shown in Fig. 4, which shows typical spectra obtained with 25 nm thick wire arrays. Notice that most of spectra shown in the following concern 25 nm thick samples, but that, indeed, for the other above mentioned thicknesses, we performed the equivalent investigations. One mode, presenting the lowest frequency (higher resonance field), appears to have characteristics strictly identical to the uniform mode occurring in a CFA unpatterned (continuous) film. The variation of its frequency versus the applied field is shown in Fig. 5a. It can be fitted through the following expression:

$$f_{\parallel} = \frac{\gamma}{2\pi}\left[\left(H + \frac{H_4}{2}\right)\left(H + \frac{H_4}{2} - H_{\perp} + H_{dem}\right)\right]^{0.5} \quad (3)$$

The appropriate gyromagnetic factor $\frac{\gamma}{2\pi} = 29.2$ GHz T^{-1}, the perpendicular anisotropy field $H_{\perp}$, the in-plane fourfold anisotropy field H_4 and the demagnetizing field $H_{dem}(=4\pi M_s)$ can be found in one of our previous publications [20] and are indicated in the figure caption. Notice that H_4, which is of magneto-crystalline origin [20], is rather large and, thus, cannot be neglected. Conversely, the weak in-plane uniaxial anisotropy field and the exchange contribution can be neglected and, consequently, do not appear in the above equation. The presence of this mode, which is labeled as the "film mode" in the following, is not clearly understood. We observe it in all the studied arrays. Notice that in some previous works concerning ferromagnetic resonance or Brillouin scattering data [17,23–25] this mode was also found. Moreover, within the frame of the dipolar approximation, it corresponds to an existing (but singular) solution [26].

The recorded spectrum also contains one or two resonance modes lying at frequencies slightly higher than that of the "film mode". We will design them as the "wire modes". Focusing on the nearest mode from the film mode, its frequency variation versus the applied field is well described by introducing in Eq. (3) an additional term taking account of the modification of the demagnetizing effects, induced by the patterning of the film in order to form a wire array

$$f_{w1\parallel} = \frac{\gamma}{2\pi}\left[\left(H + \frac{H_4}{2} + N_y H_{dem}\right)\left(H + \frac{H_4}{2} - H_{\perp} + (1 - N_y)H_{dem}\right)\right]^{0.5} \quad (4)$$

The fitted values of N_y allow for defining an effective u ($u = N_y W/d$) parameter (blue triangles in Fig. 2b), which is compared in Fig. 2b to the measured one through MOKE and to the calculated ones (u_c (red circles) and u_m (black squares)). The above simple model does not allow for treating the higher frequency wire modes, which are eventually observed in our FMR spectra (and, as discussed below, in Brillouin light scattering spectra). The simplest way to give account of the occurrence of a manifold of wire modes starts from the propagating modes in a thin film: the patterning induces a lateral

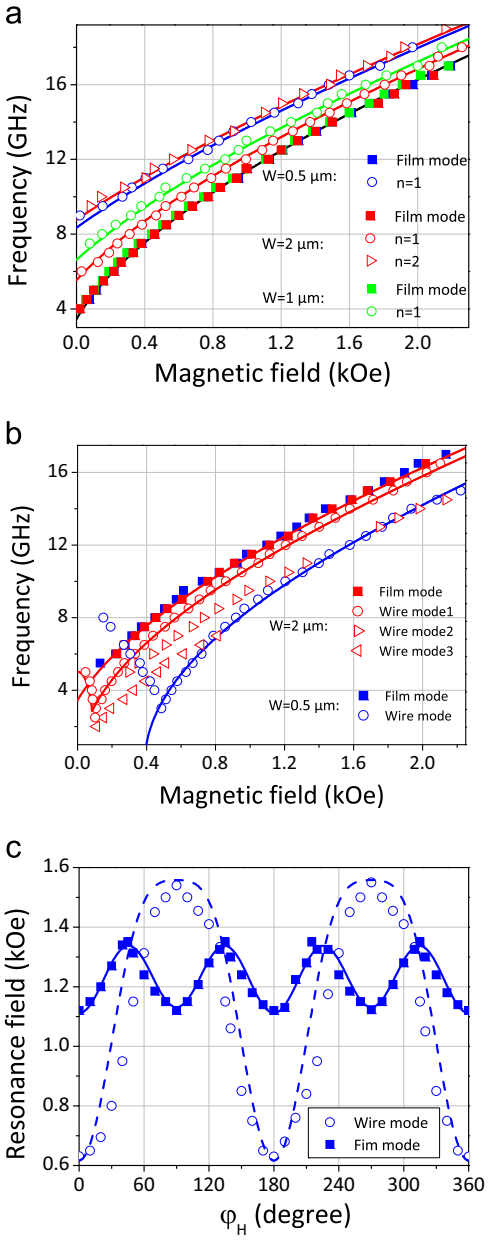

Fig. 5. Field dependence of the resonance frequencies of the observed modes in 25 nm Co_2FeAl arrays of wires with various widths. The magnetic field is applied along the wires (a) axis or (b) along their width. (c) Angular dependence of the observed resonance field of the wire and of the film modes in 25 nm Co_2FeAl arrays of wires of $W=0.5$ and $S=0.5$ μm and 12 GHz driven frequency. The solid lines refer to the fit using Eqs. (4)–(8) and (10) with $\gamma/(2\pi) = 2.92$ MHz/Oe, $H_4 = 220$ Oe, $M_s = 1000$ Oe, $H_{\perp} = 0$ Oe and $H_u = 500$, 140 and 120 Oe for $W=0.5$, 1 and 2 μm, respectively.

quantization of their wave-vector along the y-axis, which gives rise to stationary modes along y. Their expected frequencies lie around the calculated ones for propagating modes in a semi-infinite film with a wave-vector q_n in the vicinity of $n\pi/W$, where n is a positive integer. Such a model provides [26–28]:

$$f_{wn\parallel} = \frac{\gamma}{2\pi}\left[\left(H + \frac{H_4}{2} - H_{\perp} + H_{dem}\right)\left(H + \frac{H_4}{2}\right) + \frac{H_{dem}^2}{4}(1 - e^{-2q_n d})\right]^{0.5}$$
$$\simeq \frac{\gamma}{2\pi}\left[\left(H + \frac{H_4}{2} - H_{\perp} + H_{dem}\right)\left(H + \frac{H_4}{2}\right) + q_n d\frac{H_{dem}^2}{2}\right]^{0.5} \quad (5)$$

An appropriate choice of q_n gives good fits with the experimental data. It can be deduced from numerical calculations [26,29]

that q_n is given as

$$q_n = (n + a)\pi/W \tag{6}$$

In a previous paper concerning permalloy wires [26], we found: $a = -0.3$. For $n=1$, when the relative frequency variation induced by the patterning is weak, this model is equivalent to the preceding one [30], which leads to

$$a = (2/\pi)u - 1 \tag{7}$$

Notice that our classification of these laterally quantized modes starts with $n=1$ while some other authors [17,31,10,29] describe the same set of modes by starting with $n=0$, which implies that they use a value of a equal to $(2/\pi)u$. For instance, $a=-0.3$ corresponds to $u=1.1$. The values of u fitted with the experimental data, reported in Fig. 5, do not strongly differ from 1.1. In addition, when the mode $n=2$ is observed by ferromagnetic resonance, its frequency variation versus the applied magnetic field is well represented by Eq. (5) assuming that q_2 is given by Eq. (6). In addition to the above-mentioned modes the FMR spectra allow for observing perpendicular stationary spin waves (PSSW modes) which reveal magnetic excitations strongly affected by the magnetic exchange and related to a wave-vector quantized along the thickness ($p\pi/d$ where p is a positive integer). For a continuous film, the frequencies of these perpendicularly quantized modes [20]:

$$f_{PSSWp\parallel} = \frac{\gamma}{2\pi}\left[\left(H + \frac{H_4}{2} + \frac{2A_{ex}}{M_s}\left(\frac{p\pi}{d}\right)^2\right)\left(H + \frac{H_4}{2} + H_{dem} - H_{\perp} + \frac{2A_{ex}}{M_s}\left(\frac{p\pi}{d}\right)^2\right)\right]^{0.5} \tag{8}$$

In Eq. (8), A_{ex} is the exchange stiffness. In a wire array, one expects to observe PSSW modes at the following frequencies:

$$f_{w1PSSWp\parallel} = \frac{\gamma}{2\pi}\left[\left(H + \frac{H_4}{2} + N_y H_{dem} + \frac{2A_{ex}}{M_s}\left(\frac{p\pi}{d}\right)^2\right)\left(H + \frac{H_4}{2} - H_{\perp} + (1 - N_y)H_{dem} + \frac{2A_{ex}}{M_s}\left(\frac{p\pi}{d}\right)^2\right)\right]^{0.5} \tag{9}$$

Due to the large values of these frequencies our instrumental set-up gave us access to PSSW modes resonance only for the thickest studied samples. In fact, the $p=1$ mode only appears in Cr-capped 50 nm films, and it is not unambiguously possible to conclude that it corresponds to a film mode (Eq. (8)) rather than to a wire mode (Eq. (9)). Anyway the exchange stiffness constant lies around 1.5 μerg/cm [20].

3.2.2. Magnetic field along any in-plane direction

The systematic presence of a film mode is always observed for any direction of the applied field (defined by its angle φ_H with the x wire axis). Here again, the spectra contain the film mode beside at least one wire mode and, depending on the studied sample, a PSSW mode. The systematic presence of a film mode is always observed for any direction of the applied field. Here again, the spectra contain the film mode, at least one wire mode and, depending on the studied sample, a PSSW mode. The simple model based on the modification of the demagnetizing effects due to the patterning can indeed be used when the applied field is not parallel to the wire. For an in-plane magnetic field significantly larger than $H_u = N_y H_{dem}$, the magnetization is practically parallel to the applied magnetic field and it is easy to show that the frequency of the first wire mode can be approximately written as follows:

$$f_{w1\varphi} = \frac{\gamma}{2\pi}\left[\left(H + \frac{H_4}{2}(4\cos^2\varphi_H - 3) + N_y H_{dem}\right)\left(H + \frac{H_4}{2}\cos^2\varphi_H - H_{\perp} + (1 - N_y)H_{dem}\right)\cos^2\varphi_H + \left(H + \frac{H_4}{2}(4\sin^2\varphi_H - 3) - N_y H_{dem}\right)\left(H + \frac{H_4}{2}\sin^2\varphi_H - H_{\perp} + (1 - 2N_y)H_{dem}\right)\sin^2\varphi_H\right]^{0.5} \tag{10}$$

Indeed, the film mode frequency is also obtained using the above expression, but with the condition $N_y = 0$. In the case of $\varphi_H = 90°$, for which the in-plane field is perpendicular to the wire axis (configuration 2), the variations of the frequencies versus the amplitude of the magnetic field are shown in Fig. 5b for 25 nm thick wire arrays of various widths. Concerning the film mode and the first wire mode, they follow Eq. (10) using the same parameters as the fitted ones for a field applied parallel to the wires (with, indeed, $N_y = 0$ for the film mode). In Fig. 5c, we show the corresponding variations of the resonance fields versus φ_H, measured at fixed frequency (12 GHz) for wire array of $W=0.5$ μm, for both the film mode and the first wire mode. As expected, they are very different: the thin film mode resonant field shows an angular dependence with a periodicity of 90°, monitored by the four-fold in-plane anisotropy term H_4, while, for the wire mode, the periodicity is 180° and is mainly monitored by $H_u = N_y H_{dem} = u(W/d)H_{dem}$. This study of the angular variation of the resonance field allows for an improved determination of H_u (shown in Fig. 6) and therefore of u. Coming back to the case $\varphi_H = 90°$, notice that the wire mode frequency is expected to cancel at $H = H_u - H_4/2$, as observed in Fig. 5b. However, the observed softening is not complete, which prevents for a precise determination of u. For H varying from 0 to ($H_u - H_4/2$), the frequency can easily be calculated using the same formalism as in [32]: it decreases from $(\gamma/2\pi)(H_u - H_4/2)$ to 0 when H increases from 0 to ($H_u - H_4/2$). Notice that, for $H > (H_u - H_4/2)$ the wire modes frequencies lie below the film mode frequency, in contrast with the case $\varphi_H = 0°$. For such high fields, beside the first wire mode, well described using Eq. (8) with $\varphi_H = 90°$, additional wire modes are often observed, as evidenced in Fig. 5b (wire mode 1, wire mode 2,…). However, these additional features cannot be interpreted in terms of wave-vector quantization: such an approach is only valid for $\varphi_H = 0°$. The labelling of the observed modes using parallel and perpendicular wave-vector quantizations becomes irrelevant. When the applied field is not parallel to the wires, the derivation of the resonant frequencies related to these supplementary features does not follow from a simple evident estimation and needs for a numerical treatment [33,34]. However, in the case of wires with elliptic section, it can be easily shown

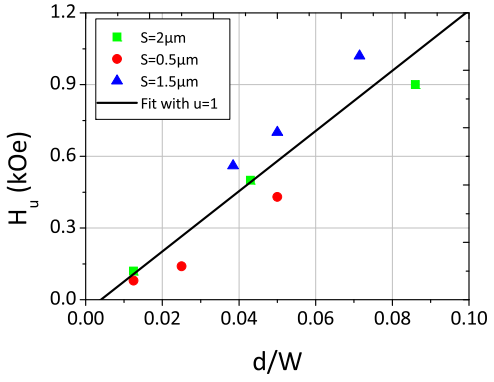

Fig. 6. Variations of the shape anisotropy field (H_u), extracted from the fit of MS-FMR measurements, as function of d/W. The solid lines are the fits using $u=1$.

[32] that, above the softening field, the uniform wire mode splits into different branches, the frequencies of which can be calculated analytically. Finally, for $\varphi_H = 90°$, here again a PSSW mode only appears in Cr-capped 50 nm films and its frequency variation versus the applied field is appropriately fitted using the above cited magnetic parameters and a perpendicular quantization with $p=1$.

3.2.3. Out-of-plane magnetic field

Our out-of-plane experimental studies were mainly performed using an applied magnetic field perpendicular to the plane of the studied sample (configurations 3 and 4). The model used in the preceding sub-section is easily adapted through the adequate permutation of the directions involved in the calculation. The equilibrium magnetization lies along the applied field when $H > (H_{dem} - H_{\perp} - H_{dem}N_y)$ (instead of: $H > H_{dem} - H_{\perp}$ in the continuous film). Then, above this field, the frequency of the first wire mode is given by

$$f_{w1\perp} = \frac{\gamma}{2\pi}\left[\left(H - H_{\perp} - (1-2N_y)H_{dem}\right)\left(H - H_{\perp} - (1-N_y)H_{dem}\right)\right]^{0.5} \quad (11)$$

Indeed, the film mode frequency is given as

$$f_{f\perp} = \frac{\gamma}{2\pi}\left[\left(H + H_{\perp} - H_{dem}\right)\right] \quad (12)$$

Taking into account that $N_y \ll 1$, it results from Eq. (11) that

$$f_{w1\perp} = \frac{\gamma}{2\pi}\left(H + H_{\perp} - H_{dem} + \frac{3H_u}{2}\right) = \frac{\gamma}{2\pi}\left(H + H_{\perp} - H_{dem} + \frac{3H_{dem}d}{2W}u\right) \quad (13)$$

In the typical experimental spectrum (Fig. 7), measured for the 25 nm thick wire array for 12.5 GHz driven frequency, the film mode and the first wire mode are always observed. We should mention that in order to increase the signal to noise ratio, the experimental set-up includes the simultaneous observation of two wires arrays having identical width but different spacing values (configuration 3). In configuration 4, two wire arrays of different widths but of common spacing value are simultaneously studied. The field-dependences of the resonance frequencies of the film mode and of the wire modes are shown in Fig. 8 for 25 nm and 50 nm-thick wires of different widths. The frequencies vary linearly with the perpendicular applied magnetic field. They allow for a determination of u, which is shown in Fig. 2b and which reasonably agrees with the other presented values. Notice that we observe additional wire modes: their frequency linearly varies versus the applied field with the same slope as the observed one for the film mode and for the first wire mode (Fig. 8). The separation from the film mode frequency of the wire mode indexed

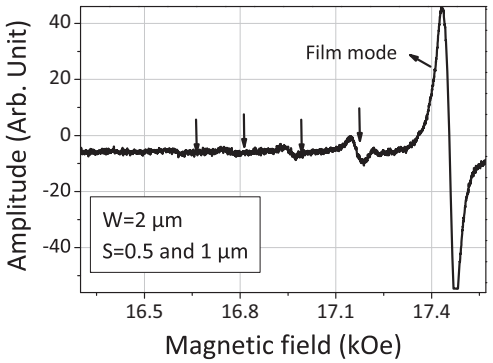

Fig. 7. MS-FMR spectra of 25 nm Co_2FeAl wire arrays measured at 12.5 GHz driven frequency. The applied magnetic field is perpendicular to the sample plane (Configuration: 3). Arrows indicate the mode positions.

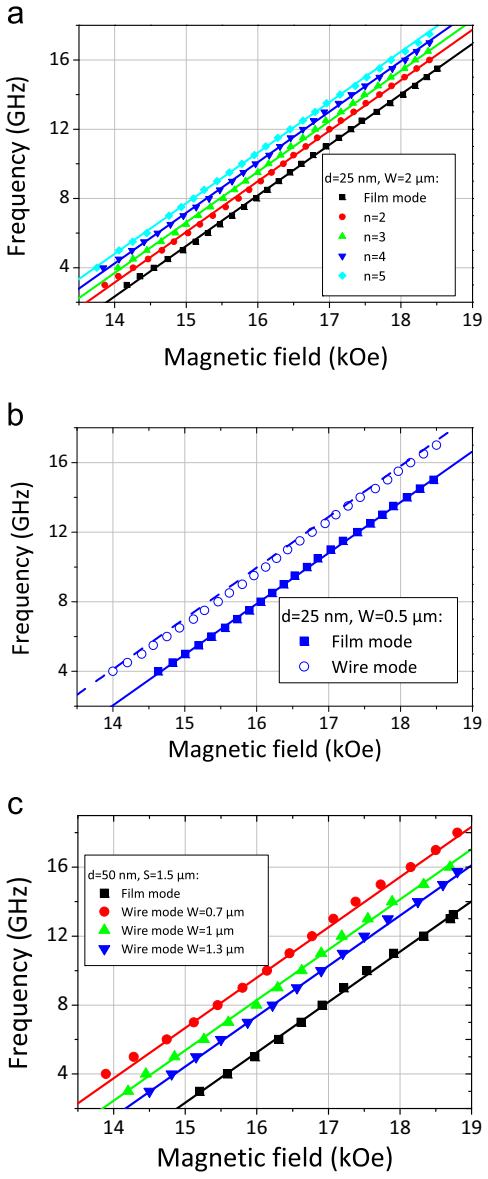

Fig. 8. Field dependence of the resonance frequency of the wire modes and of the film mode observed in Co_2FeAl arrays: (a) $d=25$ nm, $W=2$ μm, Ta capped; (b) $d=25$ nm, $W=0.5$ μm, Ta capped; (c) $d=50$ nm, various widths, Cr-capped. The applied magnetic field is perpendicular to the sample plane (configuration 3 for (a) and (b); configuration 4 for (c)). The fits are obtained using the parameters given in Ref. [20] and Eq. (13) (for (b) and (c)) or Eq. (14) (for (a)).

by n can approximately be written as

$$\Delta f_n = n\frac{\gamma}{2\pi}\frac{3H_{dem}d}{2W}u \quad (14)$$

The field separation, defined as, where H_0 refers to the film mode and where $n = 1, 2, 3\ldots$ corresponds to the successive observed modes, varies linearly versus n, as shown in Fig. 9. Except for $n=1$, the interpretation of this behavior still needs to be clarified. In the case of the 25 nm thick sample illustrated in Fig. 7, the observed series of modes seems to start with $n=2$, suggesting that the first wire mode is not detected. Consequently, for the 25-nm thick sample, we used Eq. (14) in order to derive the value of u (reported in Fig. 2), assuming that $n=1$ does not appear in the recorded spectra, which, in contrast, exhibit the modes corresponding to $n = 2, 3, 4$ and 5. As shown in Figs. 2 and 8(a), this hypothesis leads to an excellent fit associated to a very plausible value of u.

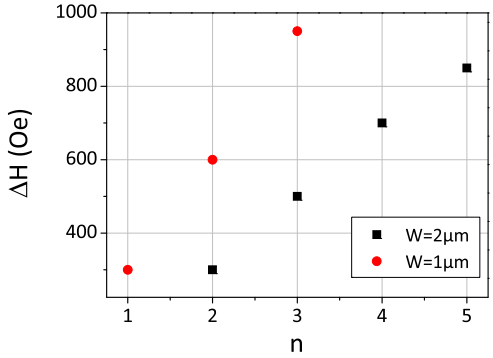

Fig. 9. Field separation ΔH (see text for definition) as function of the index (n) of the wire modes observed in 25 nm Co_2FeAl arrays of various widths.

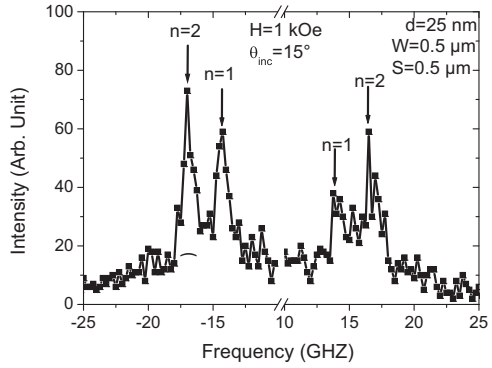

Fig. 10. BLS spectrum showing the two first wire modes ($n=1$ and $n=2$) observed in a Co_2FeAl array: $d=25$ nm, $W=0.5$ μm, $S=0.5$ μm. In-plane magnetic field of 1 kOe applied along the wires axis; back-scattering with an angle of incidence (θ_{inc}) of 15°.

3.3. Brillouin scattering

The Brillouin spectra were studied with the help of a previously described [35] experimental set-up, using a back-scattering geometry with a plane of incidence of the illuminating beam normal to the array of wires, under a varying magnetic field parallel to the wires axes. Among the thinnest (25 nm) studied wire arrays, one of them shows 2 magnetic Brillouin peaks related to the above described wire modes (Fig. 10): the model based on the wave-vector quantization, which is appropriate for the chosen geometrical arrangement provides adequate values of q_1 and q_2. We measure $(q_2 - q_1)W/\pi = 1.1$, in agreement with the expected value equal to 1. In the other samples, only one wire mode is clearly identified: using Eqs. (6) and (7), the Brillouin spectra provide an additional evaluation of u , which is reported in Fig. 2b (cyan symbols) as a function of d/W among the other determinations discussed in the previous sub-sections. In contrast with the results obtained by FMR and by Brillouin scattering concerning wires arrays of other chemical compositions [23–25], there is no trace of the film mode in the recorded spectra. Finally, Brillouin scattering due to PSSW modes is detected when the sample thickness is large enough. It appears that the interaction between the PSSW modes, strongly subjected to the magnetic exchange, and the other magnetic excitations which are treated above with the help of a purely dipolar model, is far to be negligible. A more complete theoretical approach taking into account both dipolar and exchange interactions could indeed be performed: it would allow for more rigorous results but would obscure the qualitative understanding of the effects of patterning. Moreover, the unavoidable lack of precision concerning the thickness of the films, their width, their distance and the absence of information about the roughness at the boarders of the wires, does not argue for the use of a more accurate theoretical model.

The u values, extracted form the best fits of the experimental data using the various static and dynamic techniques and summarized in Fig. 2b, reveal that those obtained by TBIIST and BLS are very close the calculated u_m and remain higher than the deduced ones from FMR measurements. In fact, in TBIIST and BLS experiments, the spot size is less than 100 μm and therefore, the hypothesis of $N_x = 0$ is fulfilled since the probed part of the wire is very small compared to the wires length (500 μm). In contrast, in MS-FMR method, the whole wires are probed and, then, the contribution of edges could result in a non-zero value of N_x.

4. Conclusion

Co_2FeAl continuous films of thickness $d=25$ nm, $d=43$ nm and $d=50$ nm were prepared by sputtering on a (001) MgO substrate and then patterned to $500 \times 500\ \mu m^2$ wire arrays of various widths (W) and different spacings. The continuous films show full in-plane and out-of-plane epitaxial growth. The magneto-optical Kerr effect magnetometry and the transverse biased initial inverse susceptibility and torque (TBIIST) methods revealed a dominant uniaxial anisotropy which increases linearly width d/W, due to the shape. The microstrip ferromagnetic resonances (MS-FMR) with magnetic fields applied along the wire axis as well as along the wire width or perpendicularly to the wire plane reveal the presence of several modes identified as the “film mode” and as the “wire modes”. These “wire modes” result from the magnetic waves confinement due to the finite wire width. The presence of the “film mode” remains to be completely interpreted. For magnetic fields applied perpendicular to the wires plane, the field separation between the resonance fields of the film and the quantized modes increases linearly with the mode index. This mode quantization is confirmed by the Brillouin light scattering observations. A large part of the experimental results can be quantitatively interpreted as resulting from the demagnetizing terms induced by the geometrical patterning. However, the presented model, simply built on the effect of the demagnetizing field, is not able to give account of all the quantized modes present in the MS-FMR spectra. When the applied magnetic field H is parallel to the wires a more complete description is used: it introduces a wave-vector quantization induced by the patterning. For the magnetic modes concerned by both approaches, the correspondence between the 2 models is easily established. When H is not parallel to the wires quantitative descriptions of the behavior of the field dependence of the observed modes still can often be performed [32].

References

[1] H. Jaffrès, A. Fert, J. Appl. Phys. 91 (2002) 8111.
[2] G. Schmidt, J. Phys. D: Appl. Phys. 38 (2005) R107.
[3] D.C. Ralph, M.D. Stiles, J. Magn. Magn. Mater. 320 (2008) 1190.
[4] K. Inomata, N. Ikeda, N. Tezuka, R. Goto, S. Sugimoto, M. Wojcik, E. Jedryka, Sci. Technol. Adv. Mater. 9 (2008) 014101.
[5] W.H. Wang, H. Sukegawa, K. Inomata, Phys. Rev. B 82 (2010) 092402.
[6] N. Weiss, T. Cren, M. Epple, S. Rusponi, G. Baudot, S. Rohart, A. Tejeda, V. Repain, S. Rousset, P. Ohresser, F. Scheurer, P. Bencok, H. Brune, Phys. Rev. Lett. 95 (2005) 157204.
[7] D. Niarchos, Sens. Actuators A 109 (2003) 166.
[8] A. Moser, K. Takano, D.T. Margulies, M. Albrecht, Y. Sonobe, Y. Ikeda, S. Sun, E. E. Fullerton, J. Phys. D: Appl. Phys. 35 (2002) R157.
[9] S.O. Demokritov, B. Hillebrands, A.N. Slavin, Phys. Rep. 348 (2001) 441.
[10] J. Jorzick, S.O. Demokritov, B. Hillebrands, M. Bailleul, C. Fermon, K. Y. Guslienko, A.N. Slavin, D.V. Berkov, N.L. Gorn, Phys. Rev. Lett. 88 (2002) 047204.
[11] K.-S. Lee, D.-S. Han, S.-K. Kim, Phys. Rev. Lett. 102 (2009) 127202.
[12] B. Lenk, N. Abeling, J. Panke, M. Münzenberg, J. Appl. Phys. 112 (2012) 083921.
[13] F. Montoncello, L. Giovannini, F. Nizzoli, P. Vavassori, M. Grimsditch, T. Ono, G. Gubbiotti, S. Tacchi, G. Carlotti, Phys. Rev. B 76 (2007) 024426.

[14] C. Bayer, J. Jorzick, B. Hillebrands, S.O. Demokritov, R. Kouba, R. Bozinoski, A. N. Slavin, K.Y. Guslienko, D.V. Berkov, N.L. Gorn, M.P. Kostylev, Phys. Rev. B 72 (2005) 064427.
[15] C.G. Tan, H.S. Lim, Z.K. Wang, S.C. Ng, M.H. Kuok, S. Goolaup, A.O. Adeyeye, N. Singh, J. Magn. Mag. Mater. 320 (2008) 475.
[16] S.-M. Chérif, Y. Roussigné, P. Moch, Phys. Rev. B 59 (1999) 9482.
[17] J. Jorzick, S.O. Demokritov, C. Mathieu, B. Hillebrands, B. Bartenlian, C. Chappert, F. Rousseaux, A.N. Slavin, Phys. Rev. B 60 (1999) 15194.
[18] C. Schoeppner, K. Wagner, S. Stienen, R. Meckenstock, M. Farle, R. Narkowicz, D. Suter, J. Lindner, J. App. Phys. 116 (2014) 033913.
[19] B.K. Kuanr, R. Lopusnik, L.M. Malkinski, M. Wenger, M. Yu, D. Scherer II, R. E. Camley, Z. Celinski, J. App. Phys. 103 (2008) 07C508.
[20] M. Belmeguenai, H. Tuzcuoglu, M.S. Gabor, T. Petrisor Jr., C. Tiusan, D. Berling, F. Zighem, T. Chauveau, S.-M. Chérif, P. Moch, Phys. Rev. B 87 (2013) 184431.
[21] M. Belmeguenai, H. Tuzcuoglu, M.S. Gabor, T. Petrisor Jr., C. Tiusan, F. Zighem, S.M. Chérif, P. Moch, J. App. Phys. 115 (2014) 043918.
[22] D. Berling, S. Zabrocki, R. Stephan, G. Garreau, J.L. Bubendorff, A. Mehdaoui, D. Bolmont, P. Wetzel, C. Pirri, G. Gewinner, J. Magn. Magn. Mater. 297 (2006) 118.
[23] S.O. Demokritov, B. Hillebrands, J. Magn. Magn. Mater. 200 (1999) 706.
[24] K. Ando, J. Ieda, K. Sasage, S. Takahashi, S. Maekawa, E. Saitoh, Appl. Phys. Lett. 94 (2009) 262505.
[25] S.-M. Chérif, Y. Roussigné, C. Dugautier, P. Moch, J. Magn. Magn. Mater. 222 (2000) 337.
[26] Y. Roussigné, S.-M. Chérif, C. Dugautier, P. Moch, Phys. Rev. B 63 (2001) 134429.
[27] C. Kittel, Phys. Rev. 73 (1948) 155.
[28] R.W. Damon, J.R. Eshbach, J. Phys. Chem. Solids 19 (1961) 308.
[29] C.T. Boone, J.A. Katine, J.R. Childress, V. Tiberkevich, A. Slavin, J. Zhu, X. Cheng, I.N. Krivorotov, Phys. Rev. Lett. 103 (2009) 167601.
[30] F. Zighem, Y. Roussigné, S.-M. Chérif, P. Moch, J. Phys.: Condens. Matter 19 (2007) 176220.
[31] C. Mathieu, J. Jorzick, A. Frank, S.O. Demokritov, A.N. Slavin, B. Hillebrands, B. Bartenlian, C. Chappert, D. Decanini, F. Rousseaux, E. Cambril, Phys. Rev. Lett. 81 (1998) 3968.
[32] Y. Roussigné, P. Moch, J. Phys.: Condens. Mater. 17 (2005) 1645.
[33] Y. Roussigné, S.-M. Chérif, P. Moch, J. Magn. Magn. Mater. 263 (2003) 289.
[34] Y. Roussigné, S.-M. Chérif, P. Moch, J. Magn. Magn. Mater. 268 (2004) 89–94.
[35] M. Belmeguenai, F. Zighem, Y. Roussigné, S-M. Chérif, P. Moch, K. Westerholt, G. Woltersdorf, G. Bayreuther, Phys. Rev. B 79 (2009) 024419.